COMMUNICATION

Precise and reversible band gap tuning in single-layer MoSe$_2$ by uniaxial strain†

Joshua O. Island,*[a] Agnieszka Kuc,[b,c] Erik H. Diependaal,[a] Rudolf Bratschitsch,[d] Herre S. J. van der Zant,[a] Thomas Heine[b,c] and Andres Castellanos-Gomez*[a,e]

We present photoluminescence (PL) spectroscopy measurements of single-layer MoSe$_2$ as a function of uniform uniaxial strain. A simple clamping and bending method is described that allows for application of uniaxial strain to layered, 2D materials with strains up to 1.1% without slippage. Using this technique, we find that the electronic band gap of single layer MoSe$_2$ can be reversibly tuned by −27 ± 2 meV per percent of strain. This is in agreement with our density-functional theory calculations, which estimate a modulation of −32 meV per percent of strain, taking into account the role of deformation of the underlying substrate upon bending. Finally, due to its narrow PL spectra as compared with that of MoS$_2$, we show that MoSe$_2$ provides a more precise determination of small changes in strain making it the ideal 2D material for strain applications.

Introduction

The two-dimensional (2D), transition metal dichalcogenides (TMDC) have attracted considerable attention in recent years.[1–5] While bulk semiconductors are quite brittle and typically break under strains larger than 1%, 2D semiconductors can withstand deformations one order of magnitude larger before rupture.[6] This large breaking strength has increased the interest in controlling the electrical and optical properties of atomically thin semiconductors by strain engineering. In the past few years many theoretical works have been devoted to the study of the role of strain on the electronic properties of semiconducting transition metal dichalcogenides.[7–18] Very recently, experimental works employing uniform uniaxial, uniform biaxial, and local uniaxial deformations have determined the role of mechanical strain on the electronic properties of atomically thin MoS$_2$, WSe$_2$, and ReSe$_2$ but the strain tunability of other members of the dichalcogenides family remains unexplored.[19–24] In particular, comparisons between two materials with a simple change in the metal (Mo *vs.* W) or chalcogenide atom (S *vs.* Se) have not been reported.

Here we employ photoluminescence (PL) spectroscopy to probe the changes in the electronic band structure of atomically thin MoSe$_2$ by uniaxial strain. Through a simple clamping and bending technique, we measure reproducible strains in MoSe$_2$ up to 1.1%. Additionally, we directly compare the photoluminescence spectra of MoSe$_2$ to that of MoS$_2$ to show that the narrow photoluminescence peak (smaller full width half maximum) allows for higher accuracy in determining small changes in strain. Upon uniform application of strain, we find that the energy of the direct band gap reduces linearly with strain by −27 ± 2 meV per percent of strain for single-layer MoSe$_2$. We carry out density-functional calculations to further support our experimental findings. By taking into account the Poisson's ratio of the underlying substrate, we calculate a band gap shift of −32 meV per percent of strain.

Sample fabrication and bending apparatus

Slippage of the flakes during the straining/relaxing cycles is a well-known problem in uniaxial straining experiments on 2D materials that severely affects the reproducibility of the results. In conventional substrate bending experiments on graphene or MoS$_2$, strain levels of ∼1% can be reliably achieved without suffering from slippage. Clamping the flake to the substrate with deposited metal electrodes has proven to be an effective method to solve the slippage issue to a great extent. In fact,

[a]*Kavli Institute of Nanoscience, Delft University of Technology, Lorentzweg 1, 2628 CJ Delft, The Netherlands. E-mail: j.o.island@tudelft.nl, andres.castellanos@imdea.org*
[b]*Engineering and Science, Jacobs University Bremen, Campus Ring 1, 28779 Bremen, Germany*
[c]*Wilhelm-Ostwald-Institut für Physikalische und Theoretische Chemie, Universität Leipzig, Linnéstr. 2, 04103 Leipzig, Germany*
[d]*Institute of Physics, University of Münster and Center for Nanotechnology, D-48149 Münster, Germany*
[e]*Instituto Madrileño de Estudios Avanzados en Nanociencia (IMDEA Nanociencia), Campus de Cantoblanco, E-28049 Madrid, Spain*
†Electronic supplementary information (ESI) available. See DOI: 10.1039/c5nr08219f

Conley *et al.* have shown reliable uniaxial straining of MoS_2 up to 2.2% by evaporating metallic bars onto the flake.[21] However, this method typically requires extra steps of cleanroom fabrication. If a shadow mask is employed instead of lithography, a careful alignment of the mask is still needed.

In this work we fabricate single-layer $MoSe_2$ samples by mechanical exfoliation of bulk crystals onto a thin poly-dimethylsiloxane (PDMS) substrate (Fig. 1(a)). Subsequently, the face of the PDMS substrate containing thin flakes is gently placed, face-down, onto a flexible polycarbonate substrate, sandwiching the flakes between the two layers. Special care is taken to place the small PDMS film on the central part of the polycarbonate strip to prevent built-in strain before measurements and for an accurate determination of the applied strain.

The PDMS film acts as a clamp to secure the flake during straining. Fig. 1(b) shows a transmission mode optical image of a $MoSe_2$ flake sandwiched between the PDMS and polycarbonate substrates (see inset of Fig. 1(b)). Single-layers can be easily distinguished from multilayer counterparts because of their strong photoluminescence yield due to the direct band gap nature of monolayer $MoSe_2$ in contrast to multilayered flakes that are indirect gap semiconductors. See the ESI† for a comparison between the photoluminescence spectra of the single layer portion of this flake (top-most part) and the bilayer region (directly below the single layer). The polycarbonate substrate is then loaded into a custom made, two-point bending apparatus shown in Fig. 1(c) and secured between two screw-posts. The moveable plateaus of the apparatus (arrow at the right-side of in Fig. 1(c)) allow full control over the bend of the polycarbonate substrate. Given the thickness (t) of the substrate (0.8 mm) and an estimation of the radius of curvature (R) for a particular strain (see ESI† for details), the strain can be estimated by $\varepsilon = t/2R$.[21,25]

Results

Fig. 2(a) shows PL spectra measured on monolayer $MoSe_2$ and MoS_2 flakes for direct comparison at strain levels of 0% and 1%. The spectra acquired for the relaxed $MoSe_2$ and MoS_2 samples (red curves in Fig. 2(a) and inset of 2(a), respectively) agree with those reported in the literature.[4,26–28] Specifically, the prominent peak at 662 nm (782 nm), determined from a Lorentzian fit, corresponds to a direct transition at the K point, giving an optical band gap of 1.59 eV (1.87 eV) for $MoSe_2$ (MoS_2).[4,26–28] It can be seen that PL peak for MoS_2 (FWHM of 46 nm) is much broader than that of the $MoSe_2$ peak (FWHM of 22 nm). Upon increasing higher uniaxial strain of 1% the PL peaks shift towards lower energy (red shift). As the exciton binding energy in transition metal dichalcogenides is expected to be nearly independent of the
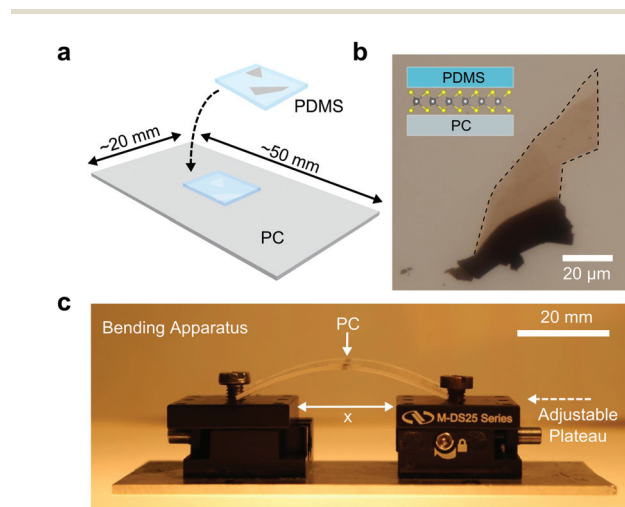
Fig. 1 (a) A viscoelastic (PDMS) stamp with exfoliated $MoSe_2$ is placed upside down onto a polycarbonate (PC) substrate to create a PC-$MoSe_2$-PDMS stack. (b) Optical transmission image of a $MoSe_2$ flake sandwiched between PC and PDMS. The inset shows a cartoon of the sandwich for a single-layer flake. (c) Optical image of the apparatus used to bend the sandwich and apply strain to the $MoSe_2$ flake.
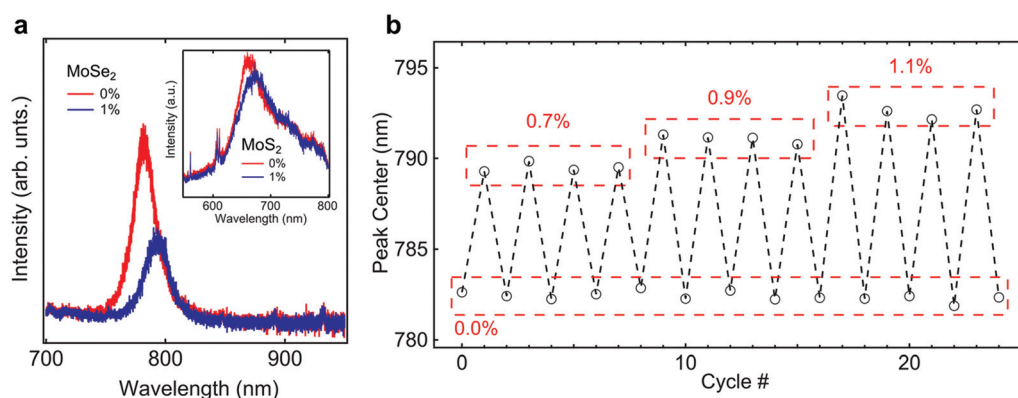
Fig. 2 (a) PL spectra for a single layer $MoSe_2$ flake at 0% and 1% strain. The inset shows the PL spectra for a single-layer MoS_2 flake at 0% and 1% strain. Note that the wavelength scale is the same width for both plots showing clearly the difference in the FWHM between the $MoSe_2$ PL peak and the MoS_2 PL peak. (b) Center of the PL peak for single-layer $MoSe_2$ as a function of strain for several straining cycles. PL shifts for strains up to 1.1% are reproducible using the simple clamp and bend apparatus in Fig. 1(c).

uniaxial strain[29] this shift of the PL emission can be directly correlated with a reduction of the band gap in the monolayer flakes. While the shift in the PL peak for $MoSe_2$ is quite clear, shifting more than one FWHM, that for MoS_2 is relatively smaller compared with the width of the peak. This suggests $MoSe_2$ as a superior material in strain applications where precise measurements of small variations in strain are required.

In order to verify that slippage is not affecting the measurements, we subjected a characteristic single layer $MoSe_2$ device to several straining/relaxing cycles. Fig. 2(b) shows the peak center, from a fit, for the $MoSe_2$ flake for repeated cycles of straining and relaxing. The PL emission reproducibly shifts from ~782 nm a uniaxial tensile strain of 0% to higher wavelengths for strains of 0.7%, 0.9%, and 1.1%. Between each cycle, the PL emission peak always comes back to the same value indicating that the flake does not slip during the measurement. By repeating this measurement at increasingly high strain levels, we determine the threshold strain value before slippage starts to play an important role. We have found that for strains higher than 1.1% these measurements are not reproducible anymore and thus we are limited to a range of strains below this threshold.

We now turn to the change in the band gap of single-layer $MoSe_2$ for given strains up to 1.1% using the described bending apparatus. Fig. 3(a) shows the shifts in the PL emission peak for a single-layer $MoSe_2$ flake for progressively increasing strain levels. The PL emission steadily shifts toward lower energies, indicating a reduction of the band gap for higher strains. Fig. 3(b) shows the change in the band gap energy for two devices. Device 1 corresponds to the PL spectra in Fig. 3(a). The change in the band gap per % of strain is extracted from the slope of a linear fit to the data for both devices. We measure a change of -27 ± 2 meV in the bad gap energy per percent strain. While reported values for the band gap change in MoS_2 are higher (~45 meV),[21] as pointed out earlier, the peak widths are broader making small variations in strain difficult to resolve. The normalized PL peak intensity is plotted as a function of strain in the inset of Fig. 3(b). We note that the peak intensity is modulated with strain but a clear direct-to-indirect bandgap transition, as reported for MoS_2,[21] could not be resolved. Johari and Shenoy suggest that such a transition would occur at strains of a factor of 2 higher than those required in MoS_2 because of the diffuse nature of the heavier chalcogenide atoms (Se).[13] Given the observed transition for MoS_2 at 1.3% strain,[21] we would expect to observe the direct-to-indirect transition at strains of roughly 2.6% which is larger than the achievable strains here.

We have employed Density-Functional Theory (DFT) to calculate the band structure of monolayer $MoSe_2$ at different strain levels (see Materials and methods for details). Fig. 3(c) shows the band structure for single-layer $MoSe_2$. We calculate a band gap of 1.35 eV including spin–orbit coupling. This value, lower than our experimentally measured value of 1.58 eV, is expected as the PBE functional is well known to underestimate the band gap energy. However, our comparative conclusions of the strained systems hold, as the band gap underestimation due to the PBE functional is the same in all cases studied here. Fig. 3(d) shows the band structure at a strain of 1.5% for armchair and zigzag strain directions which show similar changes in the band gap (see ESI† for band gap values at strains from 0% to ~2% for uniaxial strain in both directions and biaxial strain). We calculate a linear change in the band gap of -47 and -48 meV per percent of strain for the armchair and zigzag directions, respectively. Considering this deviation from the experimental shift of -27 meV per percent of strain, it is important to note the strain properties of the polycarbonate substrate itself. The polycarbonate substrate has a Poisson's ratio of ~0.37[30] at room temperature which means that an application of 1% strain along the long side of the substrate (see Fig. 1(c)) results in a contraction of 0.37% along the short side. A contraction leads to an increase in the band gap (see ESI† for band gap change with compression and strain along the armchair axis). Taking this effect into account and applying a perpendicular contraction of 0.37% for 1% uniaxial strain results in a linear band gap shift of -32 meV per percent strain (see ESI† for linear trend), improving substantially the agreement with the experimental result above.
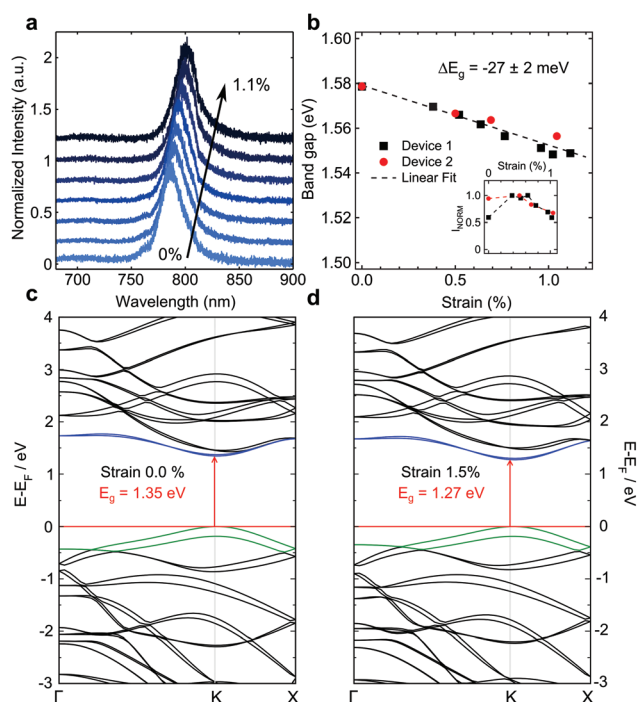
Fig. 3 (a) PL spectra for a single-layer $MoSe_2$ flake for increasing strains up to 1.1%. (b) Change in band gap for two single-layer samples (device 1 is from the spectra in (a)). The inset shows the normalized PL peak intensity for device 1 (black squares) and device 2 (red circles). (c) Calculated band structure of single-layer $MoSe_2$ including spin–orbit coupling at 0% strain and (d) at 1.5% uniaxial strain.

Conclusion

In summary, we have observed a red-shift of the PL emission of single-layer $MoSe_2$ subjected to uniform uniaxial tensile

strain, corresponding to a strain modulation of the bad gap. A simple technique is described to clamp the single-layer flakes to a bendable polycarbonate substrate and apply reproducible strains up to 1.1% without flake slippage. We find that the PL peak of $MoSe_2$ is much sharper than MoS_2 suggesting that the material would be better suited for applications of precise band-gap tuning. The experimental strain tunability of mono-layer $MoSe_2$ is found to be -27 ± 2 meV per percent of strain. The measured shift of the PL upon uniaxial strain is in good agreement with DFT calculations that predict a reduction of the band gap of -32 meV per percent of strain taking into account the Poisson's ratio of the underlying substrate. The possibility to tune the PL emission in combination with the bright and narrow PL peak of single-layer $MoSe_2$ opens opportunities to use this material for tunable optoelectronic applications.

Materials and methods

Synthesis and characterization

Bulk $MoSe_2$ material was grown by the vapor phase transport method.[31] X-ray diffraction was performed to confirm the 2H-polytype of the $MoSe_2$ single cyrstals.[27] Raman spectroscopy (not shown) and photoluminescence measurements were performed (Renishaw in *via*) in a backscattering configuration excited with a visible laser light ($\lambda = 514$ nm). Spectra were collected through a 100× objective and recorded with a 1800 lines mm^{-1} grating providing a spectral resolution of ~0.1 nm. To avoid laser-induced heating and ablation of the samples, all spectra were recorded at low power levels $P \sim$ 500 μW and short integration times (~1 s). Photoluminescence measurements however require longer integration times (~60–180 s).

Calculations

All calculations were carried out using density-functional theory (DFT) with the PBE^{32} exchange–correlation functional, with London dispersion corrections as proposed by $Grimme^{33}$ and with Becke and Johnson damping (PBE-D3(BJ)) as implemented in the ADF/BAND package.[34,35] Local basis functions (numerical and Slater-type basis functions of valence triple zeta quality with one polarization function (TZP)) were adopted, and the frozen core approach (small core) was chosen. All calculations included the scalar relativistic corrections within the Zero Order Regular Approximation (ZORA).[36–39] We have fully optimized the $MoSe_2$ monolayer (atomic positions and lattice vectors). The optimized lattice parameter of $a = 3.322$ Å was obtained for the hexagonal representation, in a good agreement with experimental data ($a = 3.288$ Å).[40] The atomic positions of $MoSe_2$ monolayer were further reoptimized for a given uniaxial or biaxial tensile strain. Electronic band gaps were obtained both from the ZORA calculations as well as from the simulations with the spin–orbit coupling (SOC). The k-point mesh over the Brillouin zone was sampled according to the Wiesenekker–Baerends scheme,[41] where the integration parameter was set to 5,

resulting in 15 k-points in the irreducible wedge. The calculated band gap of $MoSe_2$ monolayer is 1.46 and 1.35 eV from the ZORA and SOC calculations, respectively.

Acknowledgements

References

1 Q. H. Wang, K. Kalantar-Zadeh, A. Kis, J. N. Coleman and M. S. Strano, *Nat. Nanotechnol.*, 2012, **7**(11), 699–712.

2 S. Z. Butler, S. M. Hollen, L. Cao, Y. Cui, J. A. Gupta, H. R. Gutierrez, T. F. Heinz, S. S. Hong, J. Huang and A. F. Ismach, *ACS Nano*, 2013, **7**(4), 2898–2926.

3 M. Buscema, J. O. Island, D. J. Groenendijk, S. I. Blanter, G. A. Steele, H. S. van der Zant and A. Castellanos-Gomez, *Chem. Soc. Rev.*, 2015, **44**(11), 3691–3718.

4 K. F. Mak, C. Lee, J. Hone, J. Shan and T. F. Heinz, *Phys. Rev. Lett.*, 2010, **105**(13), 136805.

5 H. Fang, C. Battaglia, C. Carraro, S. Nemsak, B. Ozdol, J. S. Kang, H. A. Bechtel, S. B. Desai, F. Kronast and A. A. Unal, *Proc. Natl. Acad. Sci. U. S. A.*, 2014, **111**(17), 6198–6202.

6 R. Roldán, A. Castellanos-Gomez, E. Cappelluti and F. Guinea, *J. Phys.: Condens. Matter*, 2015, **27**(31), 313201.

7 H. Shi, H. Pan, Y.-W. Zhang and B. I. Yakobson, *Phys. Rev. B: Condens. Matter*, 2013, **87**(15), 155304.

8 M. Ghorbani-Asl, N. Zibouche, M. Wahiduzzaman, A. F. Oliveira, A. Kuc and T. Heine, *Sci. Rep.*, 2013, **3**.

9 D. M. Guzman and A. Strachan, *J. Appl. Phys.*, 2014, **115**(24), 243701.

10 H. Guo, N. Lu, L. Wang, X. Wu and X. C. Zeng, *J. Phys. Chem. C*, 2014, **118**(13), 7242–7249.

11 W. S. Yun, S. Han, S. C. Hong, I. G. Kim and J. Lee, *Phys. Rev. B: Condens. Matter*, 2012, **85**(3), 033305.

12 N. Lu, H. Guo, L. Li, J. Dai, L. Wang, W.-N. Mei, X. Wu and X. C. Zeng, *Nanoscale*, 2014, **6**(5), 2879–2886.

13 P. Johari and V. B. Shenoy, *ACS Nano*, 2012, **6**(6), 5449–5456.

14 S. Horzum, H. Sahin, S. Cahangirov, P. Cudazzo, A. Rubio, T. Serin and F. Peeters, *Phys. Rev. B: Condens. Matter*, 2013, **87**(12), 125415.

15 C.-H. Chang, X. Fan, S.-H. Lin and J.-L. Kuo, *Phys. Rev. B: Condens. Matter*, 2013, **88**(19), 195420.

16 M. Ghorbani-Asl, S. Borini, A. Kuc and T. Heine, *Phys. Rev. B: Condens. Matter*, 2013, **87**(23), 235434.

17 E. Scalise, M. Houssa, G. Pourtois, V. Afanas'ev and A. Stesmans, *Nano Res.*, 2012, **5**(1), 43–48.

18 H. Sahin, S. Tongay, S. Horzum, W. Fan, J. Zhou, J. Li, J. Wu and F. Peeters, *Phys. Rev. B: Condens. Matter*, 2013, **87**(16), 165409.

19 K. He, C. Poole, K. F. Mak and J. Shan, *Nano Lett.*, 2013, **13**(6), 2931–2936.

20 A. Castellanos-Gomez, R. Roldán, E. Cappelluti, M. Buscema, F. Guinea, H. S. van der Zant and G. A. Steele, *Nano Lett.*, 2013, **13**(11), 5361–5366.

21 H. J. Conley, B. Wang, J. I. Ziegler, R. F. Haglund Jr., S. T. Pantelides and K. I. Bolotin, *Nano Lett.*, 2013, **13**(8), 3626–3630.

22 S. B. Desai, G. Seol, J. S. Kang, H. Fang, C. Battaglia, R. Kapadia, J. W. Ager, J. Guo and A. Javey, *Nano Lett.*, 2014, **14**(8), 4592–4597.

23 G. Plechinger, A. Castellanos-Gomez, M. Buscema, H. S. van der Zant, G. A. Steele, A. Kuc, T. Heine, C. Schüller and T. Korn, *2D Mater.*, 2015, **2**(1), 015006.

24 S. Yang, C. Wang, H. Sahin, H. Chen, Y. Li, S.-S. Li, A. Suslu, F. M. Peeters, Q. Liu and J. Li, *Nano Lett.*, 2015, **15**(3), 1660–1666.

25 T. Mohiuddin, A. Lombardo, R. Nair, A. Bonetti, G. Savini, R. Jalil, N. Bonini, D. Basko, C. Galiotis and N. Marzari, *Phys. Rev. B: Condens. Matter*, 2009, **79**(20), 205433.

26 G. Eda, H. Yamaguchi, D. Voiry, T. Fujita, M. Chen and M. Chhowalla, *Nano Lett.*, 2011, **11**(12), 5111–5116.

27 P. Tonndorf, R. Schmidt, P. Böttger, X. Zhang, J. Börner, A. Liebig, M. Albrecht, C. Kloc, O. Gordan and D. R. Zahn, *Opt. Express*, 2013, **21**(4), 4908–4916.

28 S. Tongay, J. Zhou, C. Ataca, K. Lo, T. S. Matthews, J. Li, J. C. Grossman and J. Wu, *Nano Lett.*, 2012, **12**(11), 5576–5580.

29 J. Feng, X. Qian, C.-W. Huang and J. Li, *Nat. Photonics*, 2012, **6**(12), 866–872.

30 C. Siviour, S. Walley, W. Proud and J. Field, *Polymer*, 2005, **46**(26), 12546–12555.

31 R. Späh, U. Elrod, M. Lux-Steiner, E. Bucher and S. Wagner, *Appl. Phys. Lett.*, 1983, **43**(1), 79–81.

32 J. P. Perdew, K. Burke and M. Ernzerhof, *Phys. Rev. Lett.*, 1996, **77**(18), 3865.

33 S. Grimme, *J. Comput. Chem.*, 2006, **27**(15), 1787–1799.

34 G. Te Velde and E. Baerends, *Phys. Rev. B: Condens. Matter*, 1991, **44**(15), 7888.

35 *BAND2012, SCM, Theoretical Chemistry*, Vrije Universiteit, Amsterdam, The Netherlands, http://www.scm.com.

36 P. Philipsen, E. Van Lenthe, J. Snijders and E. Baerends, *Phys. Rev. B: Condens. Matter*, 1997, **56**(20), 13556.

37 E. van Lenthe, E.-J. Baerends and J. G. Snijders, *J. Chem. Phys.*, 1993, **99**(6), 4597–4610.

38 E. van Lenthe, A. Ehlers and E.-J. Baerends, *J. Chem. Phys.*, 1999, **110**(18), 8943–8953.

39 M. Filatov and D. Cremer, *Mol. Phys.*, 2003, **101**(14), 2295–2302.

40 R. Coehoorn, C. Haas, J. Dijkstra, C. Flipse, R. De Groot and A. Wold, *Phys. Rev. B: Condens. Matter*, 1987, **35**(12), 6195.

41 G. Wiesenekker and E. Baerends, *J. Phys.: Condens. Matter*, 1991, **3**(35), 6721.